MODELLING OF CLOUD, RADIATION, AND SURFACE INTERACTIONS

E. Roeckner and M. Ponater
Meteorologisches Institut der Universität Hamburg
Hamburg, F.R. Germany

1. INTRODUCTION

Particular care for the treatment of cloud and radiation has to be taken in general circulation models that are destined to simulate climate variability and climate change. For a credible assessment of the net effect arising from enhanced atmospheric greenhouse gas concentrations, the cloud-radiation interactions should be modelled reasonably well. At the same time, it is desirable to simulate the control climate (used as the reference for climate change experiments) as realistic as possible. This applies particularly for those processes for which a dependence of climate sensitvity on the simulated control climate is very likely, for example, sea-ice and cloud formation. The focus of the present paper is on cloud and radiation, and it will be demonstrated how the requirements mentioned above have been met for the respective quantities in the ECHAM/T21 model which is a climate version of the ECMWF model. After a description of the model and its particular physical schemes (section 2), we will give a brief account of the model's fidelity to simulate the observed cloud-radiation distribution (section 3). In section 4, the sensitivity of the model atmosphere to prescribed ENSO-type sea surface temperature anomalies will be discussed, again with focus on cloud and radiation.

2. MODEL PHYSICS

The model used for the present study is a low-resolution (T21) climate version of the ECMWF model (ECHAM) which is jointly run by the Max-Planck-Institute for Meteorology and the Meteorological Institute of Hamburg University. The model physics is based on the cycle 31 version of the ECMWF model including a number of modifications (Roeckner et al., 1989).

At low resolution (T21), the gravity wave drag parameterization is switched off, and a "mean" (i.e., area-averaged) orography is used. The pressure gradient force is reformulated (Simmons, personal communication) which results in a considerable reuction of truncation error over steep terrain.

Horizontal diffusion is applied only at high wavenumbers (Laursen and Eliasen, 1989). The heat transfer in the soil is simulated in a 5-layer model with a total depth of 10m and a zero heat flux condition at the bottom. Soil hydrology is parameterized in a new scheme developed from catchment considerations. Cloud processes, including subgrid-scale effects and microphysics, are simulated on the basis of the cloud water transport equation with a temperature dependent partitioning of liquid water and ice. Radiative transfer is calculated from a two-stream approximation using a broad band model with six spectral intervals in the terrestrial part (Rockel et al., 1986) and four intervals in the solar part (Hense et al., 1982). The cloud water content predicted by the prognostic cloud scheme is used to parameterize the cloud optical properties according to the suggestion of Stephens (1978).

The model has been integrated over 23 annual cycles with climatological sea surface temperatures and sea ice limits. Results will be presented from the last 20 years of the integration. In a second experiment, observed monthly mean SST for the years of 1970-1988 have been prescribed. This run will be used as a reference for the ENSO experiments discussed in section 4.

3. CLOUD AND RADIATION: TIME-MEAN STATE

The Earth's climate system is controlled by the radiation budget at the top of the atmosphere. In a steady thermodynamic state, the heating due to the absorption of solar radiation is balanced by the cooling due to the long-w ave emission to space. Any perturbation of this balance initiates a climate change. Apart from the major greenhouse gas, water vapour, the most important regulators of the planetary radiation budget are clouds. In contrast to water vapour, however, their contribution to the radiation budget is twofold: Clouds cool the planet by reflecting approximately 15% of the incoming solar radiation to space. On the other hand, clouds heat the planet because they absorb longwave radiation emitted by the Earth's surface which is generally warmer than the cloud tops. Estimates based on satellite data and GCM simulations agree that the cloud albedo effect dominates over the cloud greenhouse effect which means that for the present climate state the global mean radiative effect of clouds is a cooling of the planet.

A convenient measure of the cloud contribution to the planetary radiation budget is the so-called cloud radiative forcing (Ramanathan et al., 1989)

which is defined as the difference between the clear-sky and the total top-of-atmosphere radiative fluxes. The longwave (LWCF) and shortwave (SWCF) components of the cloud radiative forcing are defined as

$$LWCF = F_{clr} - F \quad (1)$$

$$SWCF = Q(\alpha_{clr} - \alpha_p) \quad (2)$$

where F is the total outgoing longwave flux, Q is the incoming solar radiation, F_{clr} the longwave clear-sky flux, α_p the planetary albedo, and α_{clr} the clear-sky albedo. The sum of (1) and (2) is defined as the net cloud radiative forcing

$$NCF = LWCF + SWCF \quad (3)$$

A change of the global mean cloud radiative forcing caused by a climate perturbation is called cloud feedback. Present GCMs disagree not only on the magnitude but even on the sign of the cloud feedback which causes a threefold variation of climate sensitivity for an ensemble of 16 GCMs (Cess et al., 1989). Hence, an adequate simulation of the cloud radiative forcing is a prerequisite for a reliable assessment of climate sensitivity to external forcings (CO_2 etc.).

Quantitative estimates of the global distribution of the cloud radiative forcing are available from the spaceborne Earth Radiation Budget Experiment (ERBE) launched in 1984. However, only a limited amount of ERBE data has been processed so far, and the following validation of the ECHAM simulation is based on the first ERBE year (FEB '85 - JAN '86). As apparent from Table 1 (clear-sky-fluxes) and Table 2 (cloud radiative forcing), the simulated global and seasonal mean fluxes at the top of the atmosphere are very close to the ERBE estimates. Since the accuracy of the ERBE data is 10 W/m^2 for a 2.5^o x 2.5^o area, and approximately 5 W/m^2 for the global mean, the simulated fluxes are within the band of observational uncertainty.

	SW clear-sky		LW clear-sky		NET clear-sky	
Season	ERBE	ECHAM	ERBE	ECHAM	ERBE	ECHAM
MAM	284.4	281.9	264.8	263.5	19.6	18.4
JJA	281.3	279.1	268.0	267.3	13.3	11.8
SON	288.4	288.0	266.2	263.9	22.2	24.1
DJF	295.6	293.9	261.0	260.9	34.6	33.0
ANN	287.4	285.7	265.0	263.9	22.4	21.8

Table 1: Global mean planetary radiation budget for the clear-sky part of the Earth. The ERBE data refer to the period FEB '85 - JAN '86

	SWCF		LWCF		NCF	
Season	ERBE	ECHAM	ERBE	ECHAM	ERBE	ECHAM
MAM	-45.5	-47.9	31.2	30.1	-14.3	-17.8
JJA	-46.1	-48.1	29.5	29.7	-16.6	-18.4
SON	-49.1	-48.8	30.9	28.7	-18.2	-20.1
DJF	-50.5	-48.7	29.2	27.6	-21.3	-22.4
ANN	-47.8	-48.7	30.2	29.0	-17.6	-19.7

Table 2: As Table 1, but for cloud radiative forcing

This applies for the global mean but not for a regional comparison. Figure 1 shows a comparison of zonally averaged clear-sky and total fluxes for the months of January and July. According to the definitions (1) and (2), the cloud radiative forcing is just the difference between the upper curves and the lower ones. Although the overall simulation is quite successful, a few problems are apparent. There is a lack of low-level cloudiness over the mid-latitude oceans in summer, resulting in a solar flux error of up to 50 W/m^2 near 60°S in January (upper panel). Similar errors are found over the northern hemisphere oceans in July (not shown). Moreover, there is a persistent overestimation of the solar cloud radiative forcing and an underestimation of the longwave cloud radiative forcing in the tropical

convection areas which points to problems of the vertical cloud distribution.

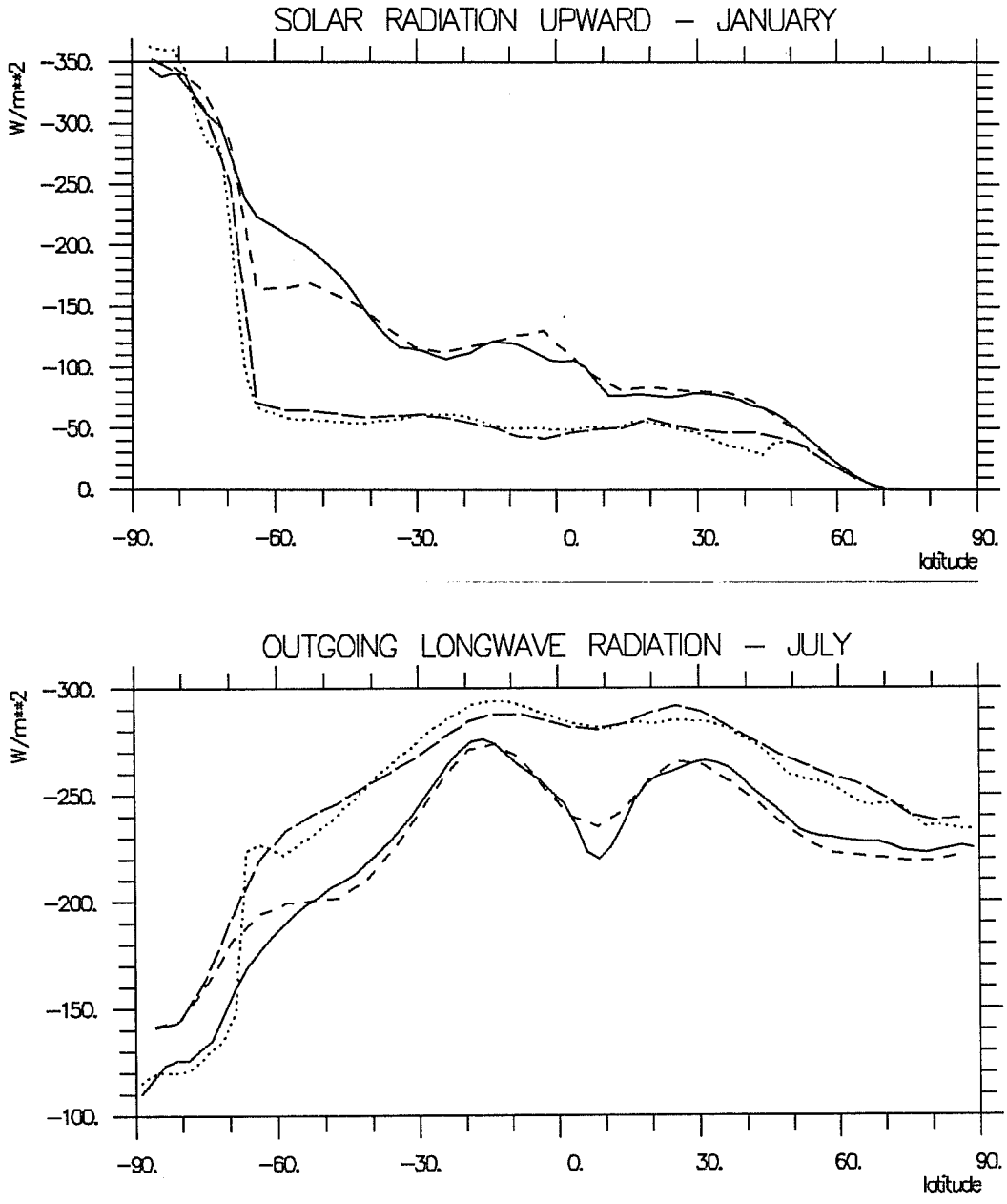

Figure 1: Comparison of zonally averaged top-of-atmosphere total and clear-sky fluxes between the ECHAM simulation (dashed curves) and ERBE data (Feb '85 - Jan '86). Top: Reflected solar radiation for clear-sky (lower pair of curves) and for the total globe (upper pair) in January. Bottom: Outgoing longwave radiation in July for clear-sky conditions (upper pair) and for the total globe (lower pair). The full and dotted curves refer to ERBE data.

The longwave flux error of approximately 20 W/m^2 over Antarctica is caused by a general lack of wintertime water vapour over polar regions.

Although the cloud radiative forcing is a useful and convenient diagnostic tool, there is some ambiguity left, apart from the vertical cloud distribution, because even in the simple case of a homogeneous cloud layer which covers a fraction C of the respective area, the cloud radiative forcing is a function of three parameters, i.e., fractional cloudiness C, clear-sky flux F_{clr}, and overcast flux F_{ovc}. The longwave component, for example, may be written as

$$LWCF = F_{clr} - F = C(F_{clr} - F_{ovc}) \qquad (4)$$

Thus, in addition to F_{clr}, either the fractional cloud cover or the overcast flux should be compared with observations in order to avoid the possibility of error compensation. A suitable dataset will be available from the International Cloud Climatology Project (ISCCP) which aims to provide monthly mean cloud data, among other products, from April 1983 to the present. Since these data are presently not available to us, we show as an example the zonally averaged total cloud cover obtained from the model simulation as compared to NIMBUS 7 data (Stowe et al., 1989) for the month of July 1983 (Figure 2). Although the basic structure is well captured by the model, there is a lack of cloudiness near 20°S, and the depression belt around Antarctica, indicated by large cloudiness, is shifted to the north.

The global distribution of the energy fluxes at the Earth's surface is still somewhat uncertain because observation from space is still in its infancy, and the coverage with conventional data based on direct or indirect estimates is very poor. Hence, the comparison of the simulated and observed net radiation budget at the surface (Figure 3) may not be very meaningful. Nevertheless, the most prominent model deviation, i.e. the somewhat high values over the summertime oceans, is consistent with a lack of shortwave cloud radiative forcing over the oceans in the summer hemispheres (c.f., Figure 1).

In summary, although the model shows some skill in reproducing the major features of the observed cloud and radiation distribution, several problems

are apparent which may be related in most cases to the inadequate modelling of maritime stratus clouds during undisturbed conditions.

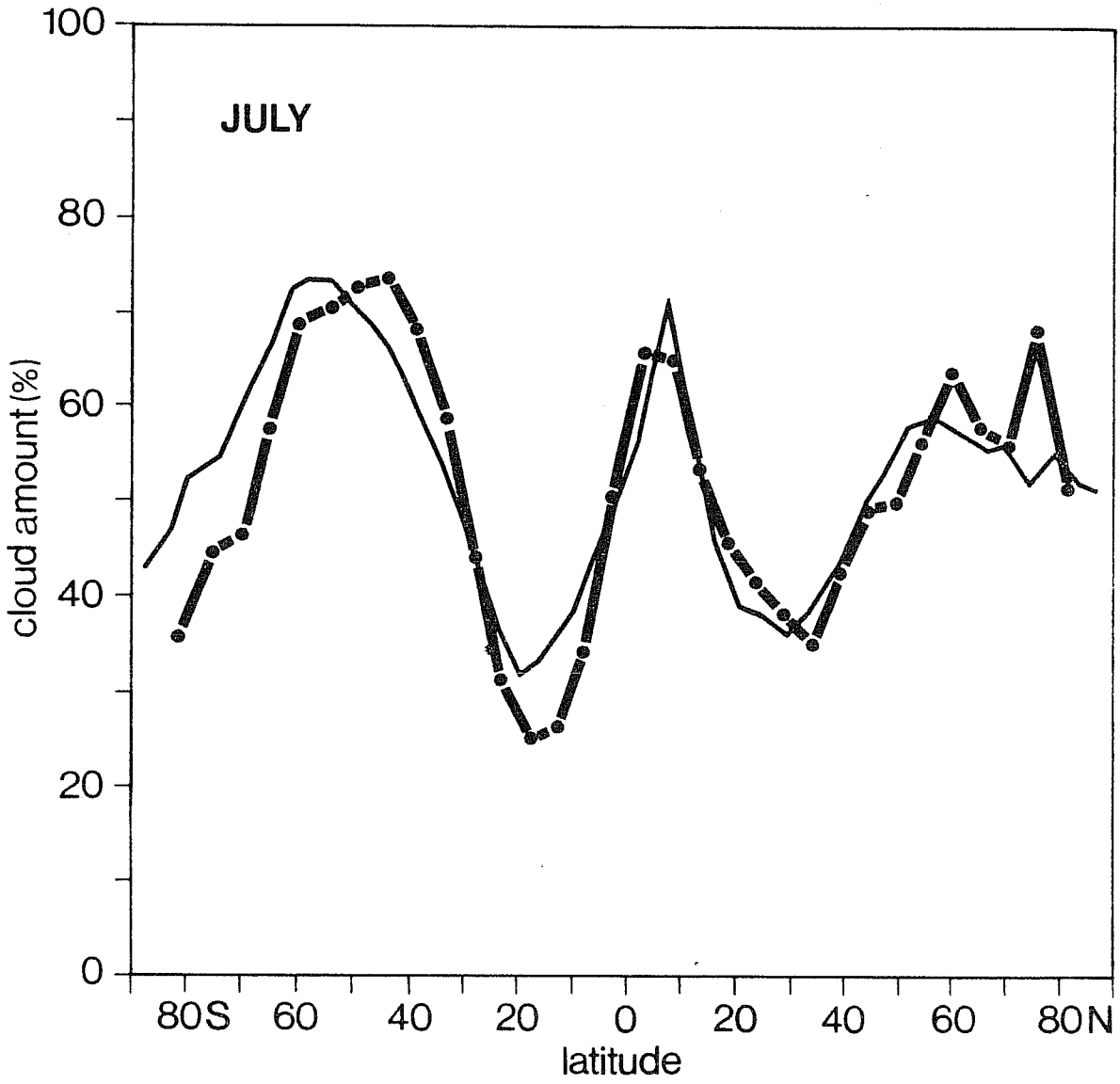

Figure 2: Zonally averaged total cloud amount according to NIMBUS 7 data (Stowe et al., 1989) for July 1983, in comparison to the ECHAM simulation (dots).

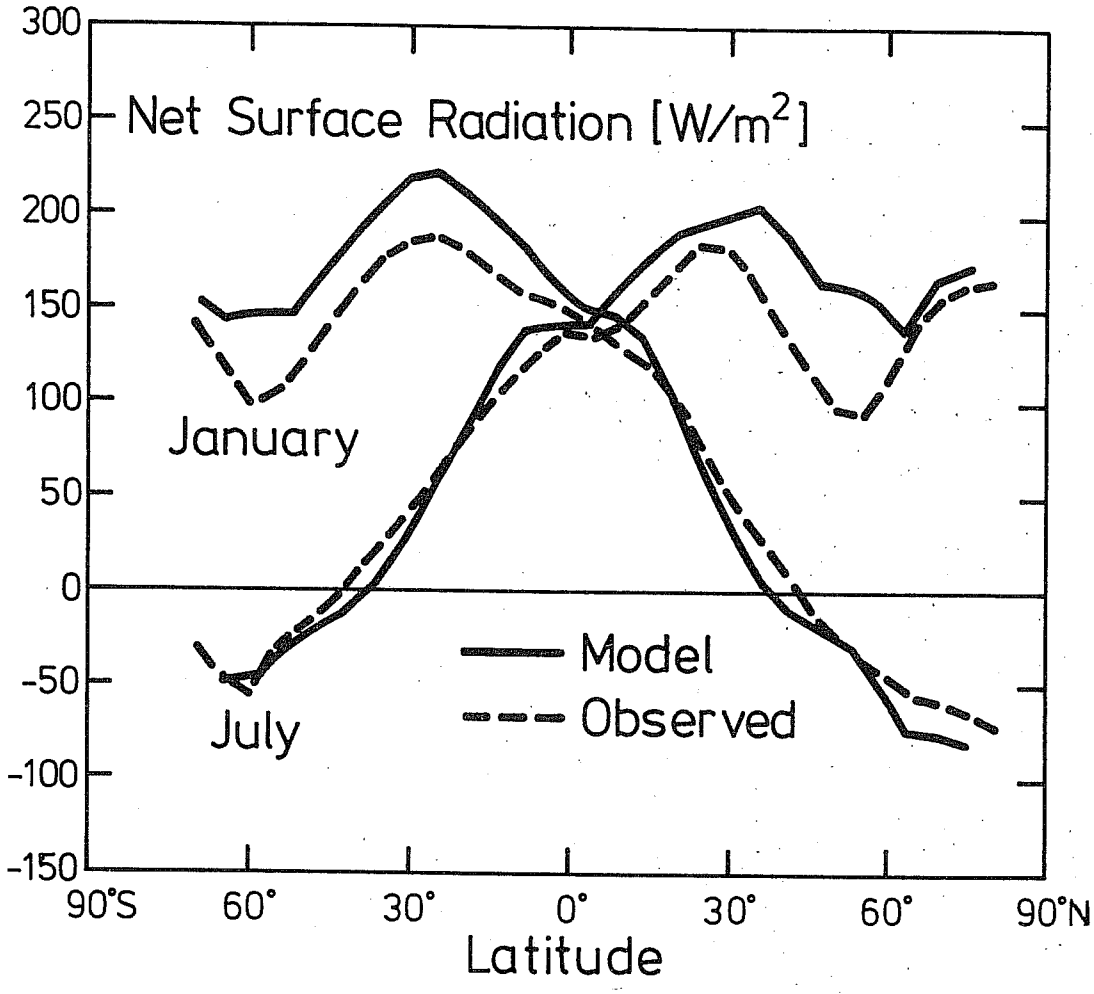

Figure 3: Comparison of zonally averaged net surface radiation budget as obtained from the ECHAM simulation (full curves) and observations according to the analysis of Esbensen and Kushnir (1981), oceans only.

4. RESPONSE TO ENSO-TYPE ANOMALIES

The development of the atmospheric response to prescribed tropical SST anomalies may illustrate how closely cloud and radiation parameters are linked to ENSO events. The reference climate was obtained from an integration with prescribed monthly SST data for the period 1970-1988. Secondly, the 1982/83 warm ENSO event was studied on the basis of five additional 9-month integrations, starting from different initial conditions obtained from the reference experiment for July 1. Thus, the ENSO ensemble consists of six realizations, one taken from the reference experiment and five from the episode runs. The signal is calculated for the three winter months, i.e., the DJF ensemble average is compared with the reference climate.

According to a simple Student-t-test, all of the response pattern shown in the next figures are significant at the 99% level for most of the tropical Pacific.

The model's response to the warm SST anomaly during 1982/83 (Figure 4) is consistent with previous observational and GCM studies. There is a significant increase of cloudiness over the warm water and a decrease of outgoing longwave radiation (Figure 5). Similarly, precipitation and column water vapour content are enhanced (Figure 6). Structure and strength of the simulated water vapour change compare well with the observed signal obtained from the analysis of satellite measurements (Prabhakara et al., 1985). To the south (extending from Australia to 120°W) and to the north (over the whole Pacific) of the region of enhanced convective activity, cloudiness and precipitation are diminished as a result of compensating subsidence.

The local response is also characterized by a considerable shift of the convective cloud tops (up to 5 km) and significant changes of the cloud radiative forcing (Figure 7).

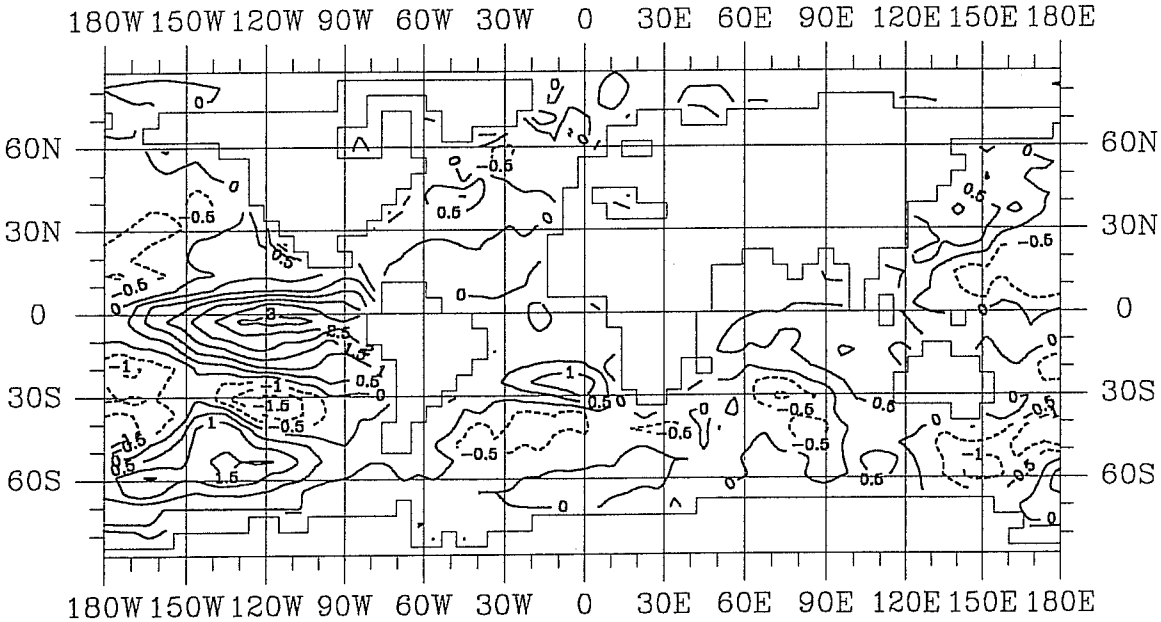

Figure 4 : Sea surface temperature anomaly (K) associated with the 1982/1983 warm ENSO event with respect to the GAGO reference run (see text). An average over the DJF-season is shown.

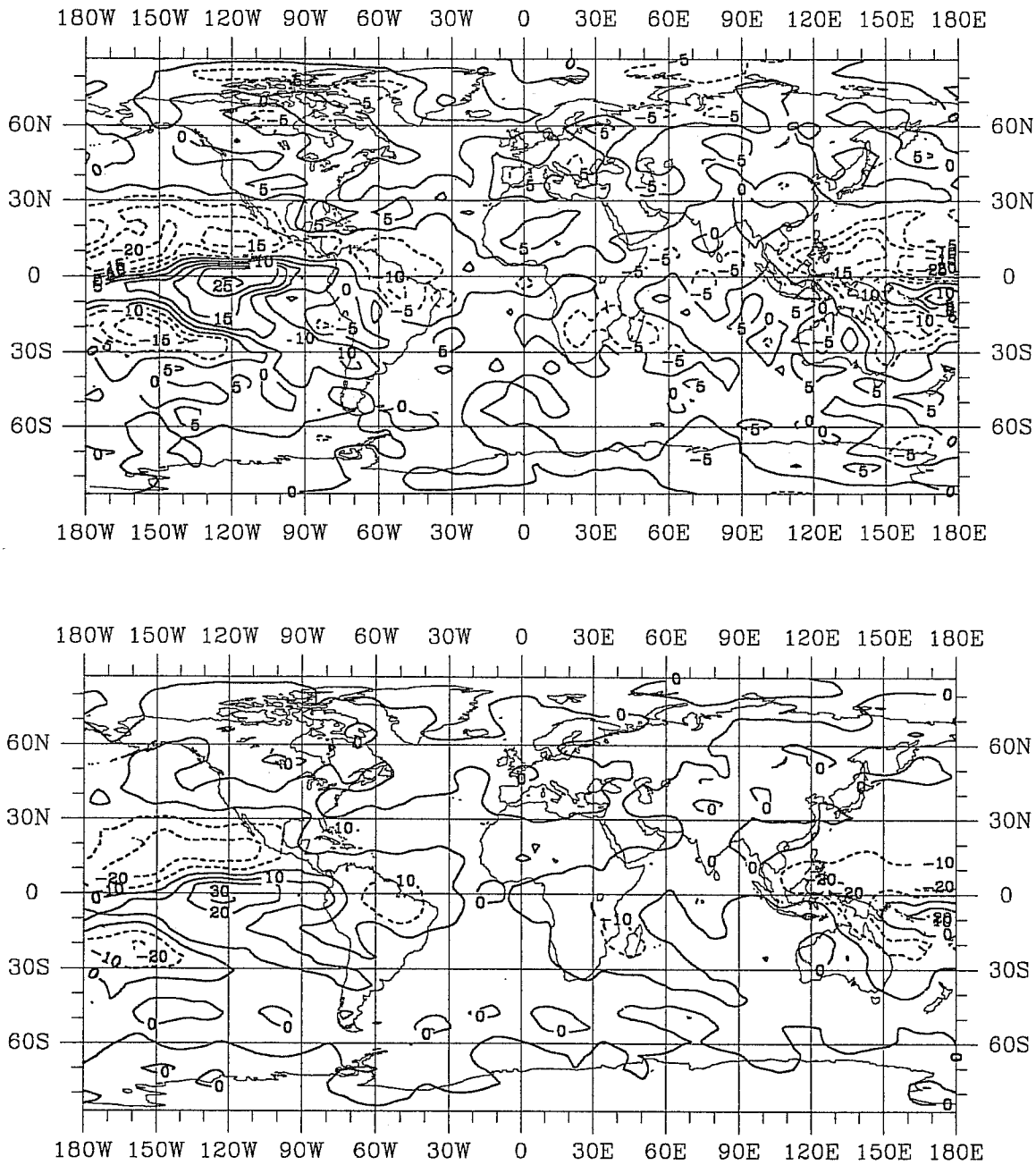

Figure 5: Difference between the six realizations of the warm ENSO event and reference run with respect to cloud cover (top panel, in %) and with respect to OLR (bottom panel, in W/m^2). The response is 99%-signifikant in practically the whole tropical Pacific between 20°S and 20°N.

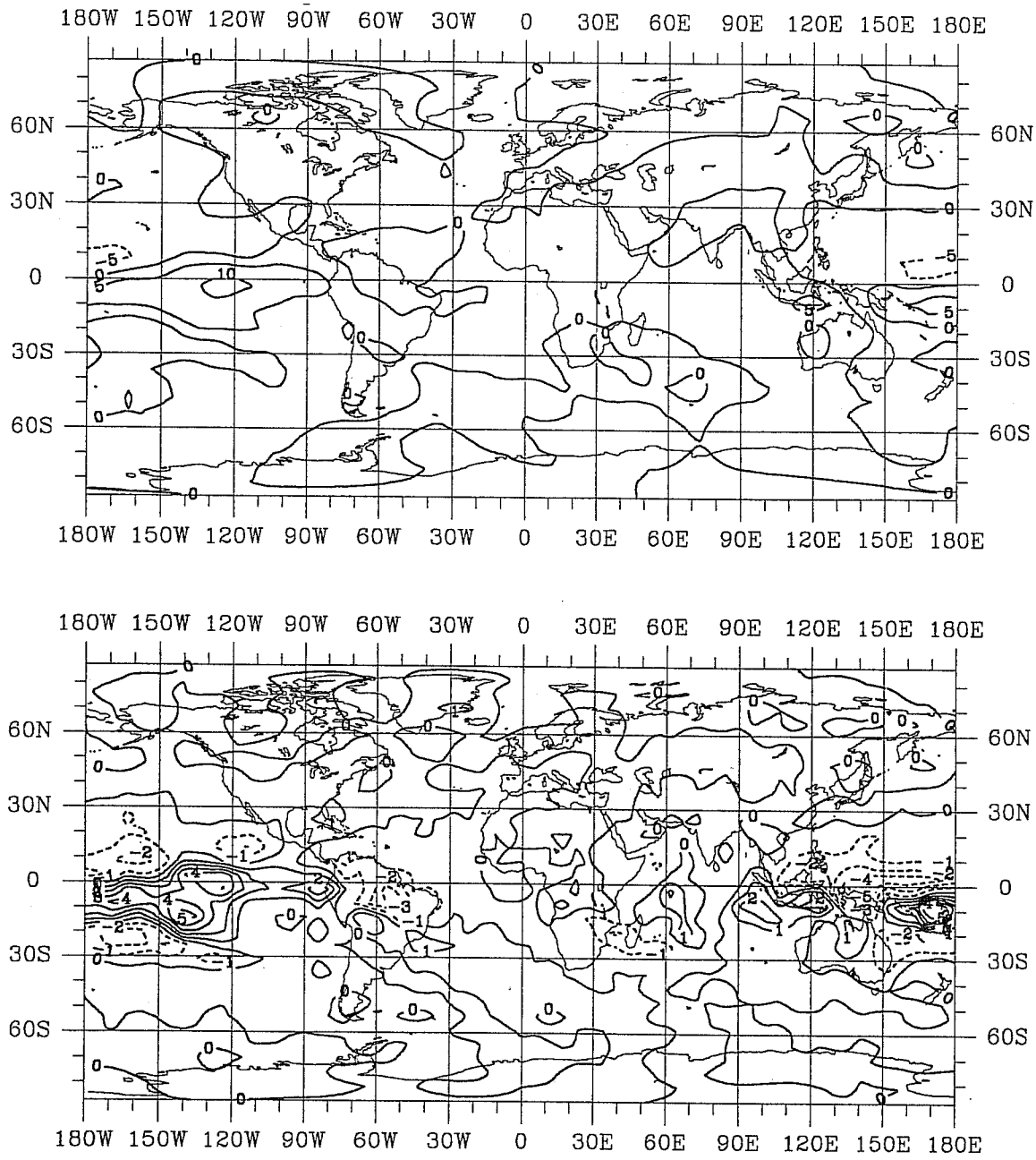

Figure 6 : Difference between the six realizations of the warm ENSO event and the reference run with respect to atmospheric water vapour content (top, in kg/m^2) and with respect to precipitation (bottom, in mm/day). The response in the tropical Pacific region between 15^{o}S and 15^{o}N is generally classified to be 99%-significant.

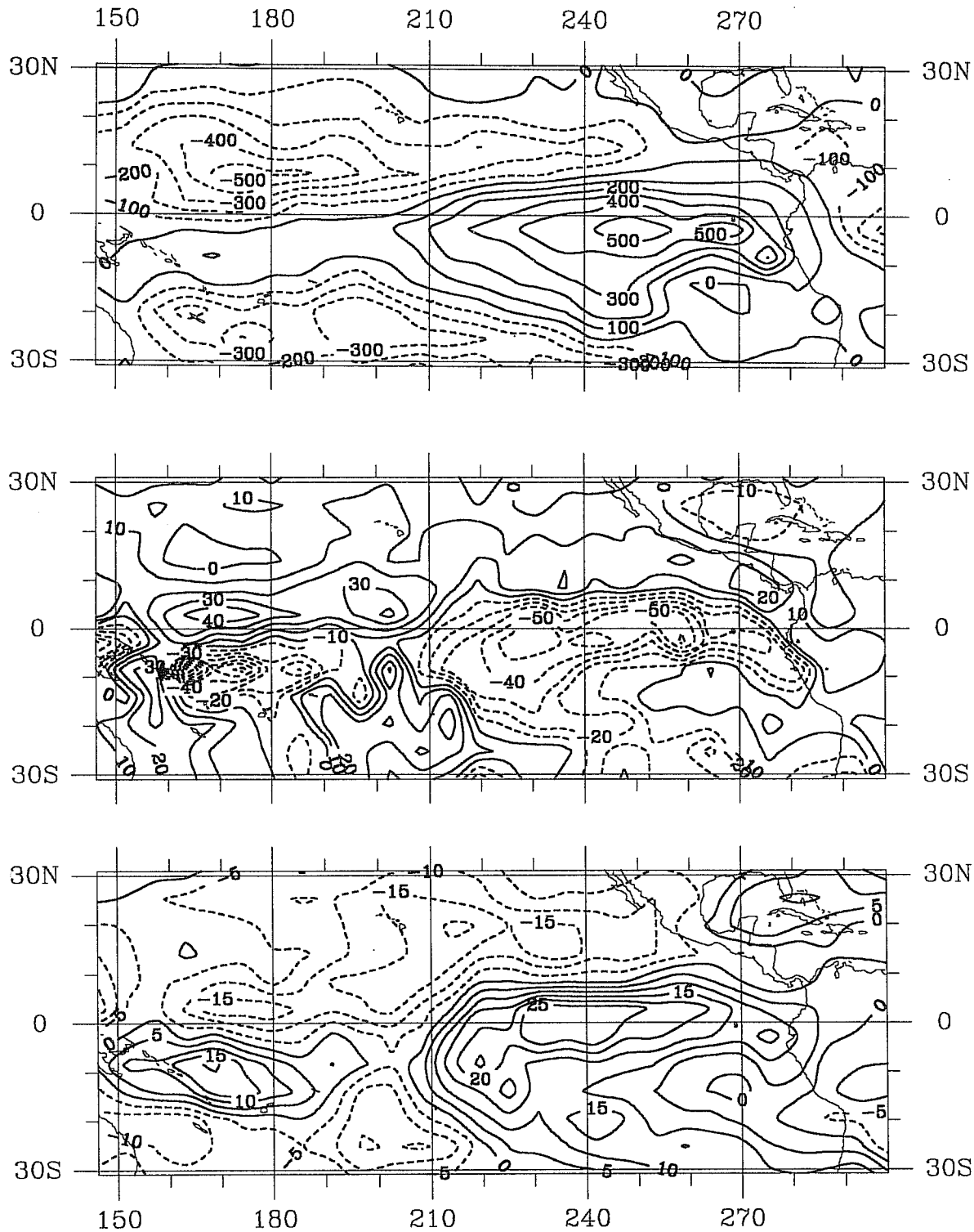

Figure 7 : Differences between the six realizations of the warm ENSO event and the reference run for the tropical Pacific region. Upper, intermediate, and lower panel show maximum convective cloud height (dam), solar cloud forcing (W/m^2), and longwave cloud forcing (W/m^2), respectively.

The net cloud radiative forcing change is negative since the increase of the cloud albedo effect over the warm water is larger than the increase of the cloud greenhouse effect. However, the vertical distribution of the two components is quite different (not schown). Whereas the cloud albedo effect is felt only at the surface,thus damping the SST perturbation (in the real world), the additional cloud greenhouse effect is felt predominantly in the atmosphere, particularly in deep convection regions (Slingo and Slingo, 1988). Thus, in addition to the larger condensational heating, the enhanced longwave cloud radiative forcing contributes to the significant warming of the whole tropical belt above 850 hPa (not shown).

5. CONCLUSIONS

Based on a comparison with the first year of ERBE data, the ECHAM model shows a considerable skill in reproducing the global mean clear-sky radiative fluxes and the cloud radiative forcing at the top of the atmosphere. On a regional scale, the largest errors are associated with a lack of low-level cloudiness during undisturbed conditions over the summertime oceans (maritime stratus).

The simulated response to a prescribed ENSO-type SST anomaly showed a consistent pattern of enhanced cloudiness, water vapour content and precipitation over the area of the warm SST anomaly. The radiative response is characterized by an enhanced cloud albedo effect (cooling the surface), and a somewhat smaller enhancement of the cloud greenhouse effect (heating the atmosphere). Due to the design of the experiment, the simulated cloud and radiation response is largely a reaction to the prescribed SST anomaly without further consequences for the dynamics of the event. The question if cloud-radiative processes may play an active role during ENSO events requires further studies with a coupled atmosphere-ocean model.

6. References

Cess, R.D., G.L. Potter, J.P. Blanchet, G.J. Boer, S.J. Ghan, J.T. Kiehl, H. Le Treut, Z.X. Li, X.Z. Liang, J.F.B. Mitchell, J.-J. Morcrette, D.A. Randall, M.R. Riches, E. Roeckner, U. Schlese, A. Slingo, K.E. Taylor, W.M. Washington, R.T. Wetherald and I. Yagai, 1989: Interpretation of cloud-climate feedback as produced by 14 atmospheric general circulation models. Science, 245, 513-516.

Esbensen, S.K. and Y. Kushnir, 1981: The heat budget of the global oceans: An atlas based on estimates from surface marine observations, Report No. 29, Climatic Research Institute, Oregon State University, Corvallis.

Hense, A., M. Kerschgens and E. Raschke, 1982: An economical method for computing radiative energy transfer in circulation models. Quart.J.Roy. Meteor.Soc., 108, 231-252.

Laursen, L. and E. Eliasen, 1989: On the effect of the damping mechanisms in an atmospheric general circulation model. Tellus, 41A, 385-400.

Prabhakara, C., D.A. Short and B.E. Vollmer, 1985: El Nino and atmospheric water vapor.: Observations from NIMBUS 7 SMMR. J.Clim.Appl.Meteor., 24, 1311-1324.

Ramanathan, V., R.D. Cess, E.F. Harrison, P. Minnis, B.R. Barkstrom, E. Ahmad and D. Hartmann, 1989: Cloud-radiative forcing and climate: Results from the Earth Radiation Budget Experiment. Science, 243, 57-63.

Rockel, B., B. Zhao and E. Raschke, 1986: A flexible radiative transfer routine for GCMs: Infrared part. In: G.J.Boer (ed.) Research Activities in atmospheric and oceanic modelling, CAS/JSC Working Group on Numerical Experimentation, Report No. 9, WMO/TD-No. 141, 4.62-4.65.

Roeckner, E., L. Dümenil, E. Kirk, F. Lunkeit, M. Ponater, B. Rockel, R. Sausen and U. Schlese, 1989: The Hamburg version of the ECMWF model (ECHAM). In: G.J. Boer (ed.) Research Activities in atmospheric and oceanic modelling, CAS/JSC Working Group on Numerical Experimentation, Report No. 13, WMO/TD-No. 332, 7.1-7.4.

Slingo, A. and J.M. Slingo, 1988: The response of a general circulation model to cloud longwave radiative forcing. I: Introduction and initial experiments. Q.J.R.Meteorol.Soc., 114, 1027-1062.

Stephens, G.L., 1978: Radiation profiles in extendes water clouds. 2. Parameterization schemes. J.Atmos.Sci., 35, 2123-2132.

Stowe, L.L., H.Y.M. Yeh, T.F. Eck, C.G. Wellemeyer, H.L. Kyle and the NIMBUS 7 cloud data processing team, 1989: Nimbus-7 global cloud climatology. Part II: First results. J.Clim., 2, 671-709.